Biomedical Signal Processing and Control 47 (2019) 252–261

Contents lists available at ScienceDirect

Biomedical Signal Processing and Control

journal homepage: www.elsevier.com/locate/bspc

NLM based magnetic resonance image denoising – A review

Hemalata V. Bhujle*, Basavaraj H. Vadavadagi

SDM College of Engineering & Technology, Dharwad, India

ARTICLE INFO

Article history:
Received 13 January 2018
Received in revised form 10 July 2018
Accepted 27 August 2018
Available online 5 September 2018

Keywords:
Magnetic resonance
Non-local means
Denoising
Sparseness

ABSTRACT

Denoising Magnetic Resonance (MR) image is a challenging task. These images usually comprise more features and structural details when compared to other types of images. These structural details in MR images provide additional information to physicians for better diagnoses and hence there is a need to preserve these details. Over the past few years, various MR image denoising techniques have been evolved. Among them, the techniques based on Non-Local Means (NLM) have achieved excellent performance by exploiting similarity and/or sparseness among the patches. The evolution of NLM filter has changed the paradigm of research in the area of MR imaging. Many variants of NLM algorithms have been developed till today which in addition to retaining the edge/structural features, improve the signal to noise ratio and computational efficiency. The aim of this paper is to provide an exhaustive review of the published literature on NLM based MR image denoising techniques. A critical review and discussion on the advantages and limitations of these techniques are provided with quantitative result analysis.

1. Introduction

Magnetic Resonance Imaging (MRI) has emerged as a powerful technology which enables mankind a detailed and extensive study of structural features and functional characteristics of the internal organ. Information provided by MRI technique differs from other imaging modalities like ultrasound and computed tomography scanning. The ability of this technique to obtain images in multiple planes without moving the patient and its potential to characterize and discriminate among tissues based on their physical and biochemical properties offer special advantages in clinical diagnoses and surgical treatment. The application of MRI ranges from imaging static anatomy to many clinical tasks such as imaging blood vessels, cardiac imaging, measuring tissue temperature and fixing retinal disorders. The only limitation of this technique is being its spatial resolution and long acquisition time. The accuracy of the clinical diagnosis depends on the visual quality of MR images which may be seriously degraded by noise during the acquisition process. The acquisition process of MR image gets affected by different kinds of noises. In a single channel acquisition, MR signals are reconstructed by computing inverse discrete Fourier transform. The sampling of MR images is done in the frequency domain and images are extracted from both real and imaginary channels. Signals in these channels are corrupted with additive white Gaussian noise. Since magnitude computation is a nonlinear process, MRI signal follows Rician distribution [1]. Noise distribution in multichannel signal acquisition system can be described as non-central chi distribution [2,3] since MR image is reconstructed by combining complex images. In parallel imaging system, amplitude of the noise changes with the spatial location of the image and hence tends to introduce chi or Rician distributed noise [4].

Noise removal in MR images can be dealt with two ways. One way is to acquire multiple images of the same data and average them. However, this procedure is quite slow and some time introduces motion artifacts. In the second approach, suitable image denoising techniques are applied after image acquisitions which provide reliable and fast results. Various denoising filters have been proposed for MR images in the past as a post-acquisition process. A few of them include Gaussian filtering [5,6], anisotropic diffusion filtering [7,8], wavelet thresholding [9,10], bilateral [11,12] and statistical approaches [13,14]. Manjón et al. [15] were the first among to apply NLM filter [16] for MR images perturbed with Rician noise. This filter performed superior to all aforementioned filters and was treated one of the state of the art filters at that time for MR image denoising. However high computational cost of this filter has lead many researchers for future work. Presently, abundant quantities of papers can be found on NLM based MR image denoising. This paper provides the reader the review of all such recently developed techniques pertaining to MR images with critical analysis, advantages, and limitations of each technique.

The organization of the remainder of this paper is as follows. In Section 2, characteristic of noise in MRI and its estimation is given.

* Corresponding author.
E-mail address: hemalatabhujle@gmail.com (H.V. Bhujle).

https://doi.org/10.1016/j.bspc.2018.08.031
1746-8094/

In Section 3, a complete review on NLM based MR image denoising techniques are provided. In Section 4, comparative results among various published literature are provided. Section 5 concludes the paper.

2. Distribution of noise in MR data

An image is usually assumed to be corrupted with an additive white Gaussian noise, which is quite simple to deal with. However, noise in MR image is signal dependent and signal formation model changes it to Rician. Rician noise degrades the quality of the image qualitatively and quantitatively. Detectability of MR image gets drastically reduced due to bias introduced by Rician noise. In this section, we provide the reader the rationale behind Rician noise assumption.

The complex MR datum X is given by

$$X = X_{Re} + jX_{Im} \tag{1}$$

where X_{Re} and X_{Im} are real and imaginary components of the data. These components are affected by ξ_1 and ξ_2, where ξ_1 and ξ_2 are additive white Gaussian noise with zero mean and standard deviation σ.

$$X_{Re} = Scos\theta + \xi_1 \tag{2}$$

$$X_{Im} = Ssin\theta + \xi_2 \tag{3}$$

Here S is the original MR image and θ is the phase. A noisy MR image when represented as the magnitude of the noisy raw data, given by

$$|X| = \sqrt{(Scos\theta + \xi_1)^2 + (Ssin\theta + \xi_2)^2} \tag{4}$$

The distribution of $|X|$ becomes Rician [17] [1], and is represented as

$$P(X|S,\sigma) = \frac{X}{\sigma^2} e^{\frac{-(X^2+S^2)}{2\sigma^2}} I_0\left(\frac{XS}{\sigma^2}\right), \quad X > 0 \tag{5}$$

Here I_0 denotes the modified Bessel function of the first kind with order zero, S is the noiseless signal, σ^2 is the noise variance of Gaussian distribution and X is the observed MR magnitude image. From the above equation it is clearly observed that for low intensity regions i.e., when S approaches zero, the expression leads to a Rayleigh PDF given by

$$P(X|S,\sigma) = \frac{X}{\sigma^2} e^{\frac{-X^2}{2\sigma^2}}, \quad X > 0 \tag{6}$$

wherever the signal intensity is high the above PDF approaches a Gaussian distribution [18].

$$P(XS,\sigma) = \frac{1}{\sqrt{2\pi\sigma^2}} e^{\frac{-(X-\sqrt{S^2+\sigma^2})^2}{2\sigma^2}} \tag{7}$$

To estimation the noise in a magnitude image $|X|$, Nowak [18] squared the magnitude by which bias in the MR images can be made additive and signal independent.

$$|X|^2 = (Scos\theta + \xi_1)^2 + (Ssin\theta + \xi_2)^2 \tag{8}$$

Taking the expectation on both the sides yields,

$$E\left[|X|^2\right] = E[\left(Scos\theta + \xi_1\right)^2 + \left(Ssin\theta + \xi_2\right)^2 = \mu_S^2 + 2\sigma^2 \tag{9}$$

where μ_s is the mean value of the pixels. Bias in the squared magnitude domain is observed to be $2\sigma^2$. The noise in the MR image is estimated from the background regions [19]. The estimate of noise in the background is given by $\sigma = \sqrt{\frac{\mu}{2}}$ where μ is the mean value of the pixels from the background. Sijbers et.al [20–22] were the first among to estimate Rician noise in MR images using the statistical approach like Maximum Likelihood Estimation (MLE) prior to signal reconstruction and bias compensation. This work has been extended further to estimate Rician noise from the background mode of MR image histogram [23]. There are numerous recent developments in MRI, as far as fast acquisition and reconstruction of data are concerned. A closed form solution of Linear Minimum Mean Square Error (LMMSE) estimator is proposed [24] for MR images acquired with a single coil that follow a Rician model. Noise estimation in SENsitivity Encoding (SENSE) and GeneRalized Autocalibrating Partially Parallel Acquisitions (GRAPPA) reconstructed image has been discussed in [25]. A high Angular Resolution Diffusion Imaging (HARDI) and HYbrid Diffusion Imaging (HYDI) techniques are usually performed at high b values and hence yield low Signal to Noise Ratio (SNR). A noise correction scheme for such techniques is discussed in [26]. Authors in [27] have devised a scheme to estimate noise from correlated multiple coil MR data, however in [28] noise in single and multiple coil MR data is estimated by statistical models.

3. NLM based MR image denoising

For MR images, there is always a trade-off between the resolution and SNR. High-resolution images lead poor SNR and vice-versa with low resolution images. However, to detect anatomical structures images should possess good resolution with high SNR. Hence dealing with noise to obtain the best possible result is quite difficult. In this regard, NLM filter is a preferred choice as it has good edge preserving capability while denoising.

3.1. NLM filter

A nonlocal means filter [16] exploits redundancy in the image. Each pixel in NLM filtered image is the weighted average of all other pixels in the image. This can be represented as

$$\begin{aligned} NLM(I(i)) &= \sum_{j \in N_i} w(N_i, N_j) I(j) \\ 0 \le w\left(N_i, N_j\right) \le, &\sum_{j \in N_i} w(N_i, N_j) = 1 \end{aligned} \tag{10}$$

where $I(j)$ is the noisy intensity of the j^{th} pixel, N_i is the neighborhood of i^{th} pixel , $w\left(N_i, N_j\right)$ is the weight function computed based on the similarity between two patches. In [16] authors have limited search window size and patch size to 21×21 and 7×7, respectively. Euclidean distance between two patches is given by

$$d = \left\| I(N_i) - I\left(N_j\right) \right\|_{2,\sigma}^2 \tag{11}$$

where σ is the standard deviation of the Gaussian kernel. Further the weights can be computed as

$$w\left(N_i, N_j\right) = \frac{1}{Z(i)} e^{\frac{-d}{h^2}} \tag{12}$$

where h is the filtering parameter and Z is a normalization constant given by

$$Z(i) = \sum_j e^{\frac{-d}{h^2}}. \tag{13}$$

3.2. NLM denoising techniques in MRI

The variants of NLM filter developed for MR image denoising is illustrated in Fig. 1. The NLM denoising for MR image sequences can be broadly classified into four categories. There are various NLM techniques which improve the SNR with better edge preservation however, suffer from high computational cost. 3D processing of

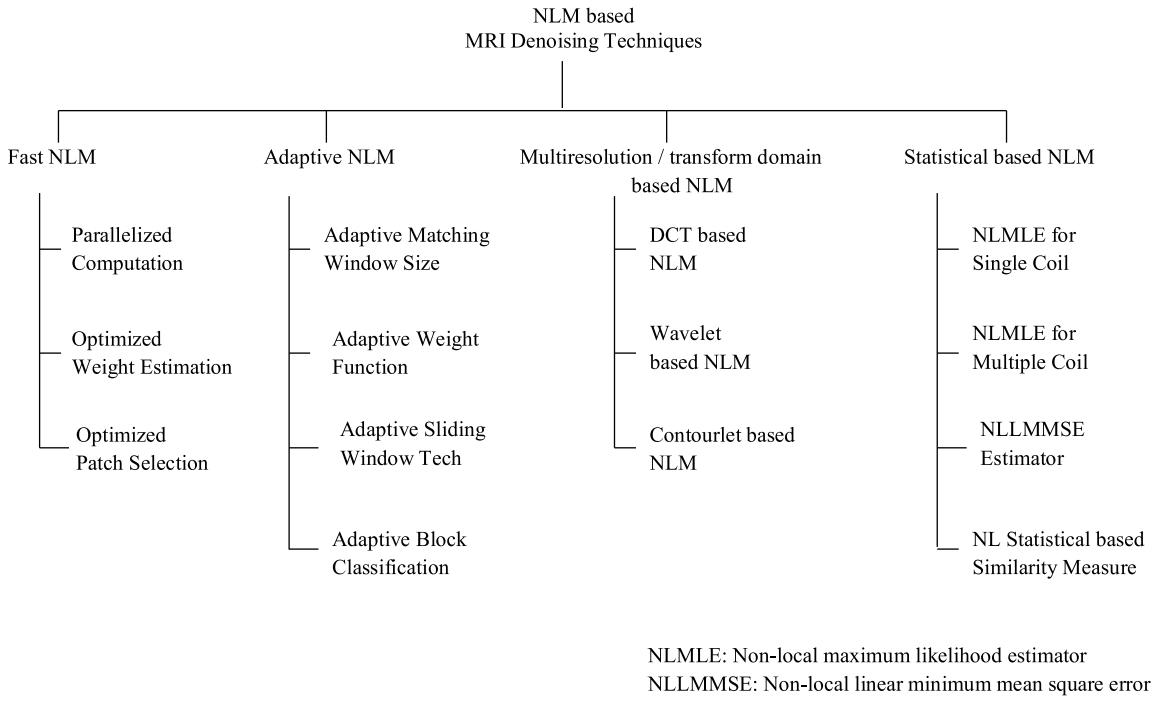

Fig. 1. Classification of NLM based MR image denoising methods.

MR imaging results in high computational cost due to the similar patch search in current and adjacent voxels of MR data. Numerous papers are available in the literature to speed-up NLM denoising which are categorized under the technique of fast NLM denoising. Second category (adaptive NLM) of papers are based on changing search window, patch size and weight function of NLM adaptively in accordance to spatially varying noise, textural pattern and edge orientation. Next category of NLM denoising exploits intrinsic properties of MR images i.e., sparseness and self-similarity in the multiresolution framework for better denoising. Multiresolution approach decomposes the image into different frequency components that help to study each component with a resolution matched to its scale. In the fourth category, NLM technique is applied in-conjunction with statistical/estimation approach for MR data that follows central and non-central χ distribution (spatially varying) due to parallel and multi-channel MRI acquisition.

The application of NLM filter for Rician perturbed MR image was initially proposed by Manjón et al. [15]. Though MR image like any other natural image possesses a high degree of redundancy in patch similarity, is quite different in terms of its fine edges and anatomical structures. This paper tried to set the optimal parameters of NLM filter to obtain high SNR with bias compensation. However, over-smoothing at some homogeneous regions resulted in degradation of the accuracy. Also, the technique is deprived of any speed-up strategy to solve the problems related to heavy computations. Weist et al. [29,30], were among the few to use NLM filter to denoise low SNR Diffusion-Weighted (DW) MR and Diffusion Tensor (DT) MR images. The algorithm works efficiently on High Angular Resolution Diffusion Imaging (HARDI) and Q Space Imaging (QSI). A very similar an unbiased nonlocal means scheme for Diffusion Weighted Imaging (DWI) filtering was proposed by Aja-Fernandez et al. [31]. All the aforementioned papers depict pioneering work in MR denoising using NLM principle. Moreover, these techniques are computationally demanding. There are large number of papers on reducing the computational cost which will be reviewed in the next section in which few while reducing computations even improve the accuracy of the filter.

3.2.1. Fast NLM techniques

Reducing the computational cost is a critical step while extending the NLM filter to 3D MR data. Most of the works in literature focus mainly on this issue. Few speed-up techniques, in addition to reducing the computational cost improve the filter accuracy. Coupé et al. [32] were the first to suggest optimized and automated NLM filter. The techniques adopted for optimization include the selection of the most relevant voxels, blockwise implementation, and parallelized computations. This paper considers only few most relevant voxels having high weights while NLM denoising which reduce the computations heavily. Parallelized computations over several processors via a cluster or a grid further reduce computational time. A very similar technique to reduce the computational time is proposed in [33] which distribute the operations on several processors via a cluster or a grid. This method is able to speed-up the NLM filter to some extent but fails to achieve higher accuracy. Hu et al. [34] proposed a structure tensor to encapsulate high order information required for optimal sampling pattern. Optimal sampling is done by selecting a small subset of voxels. The speed-up factor is directly proportional to the sampling rate. Cihui et al. [35] proposed a denoising scheme where both computational efficiency and accuracy of NLM filter have been improved. This technique removes excessive noise by introducing a preprocessing step of Gaussian filtering where weights are computed on the filtered image instead of a noisy image. Computational efficiency is achieved by optimized weight estimation by utilizing group of a square and a line as the neighbor instead of the original cubic neighbor.

Run-time efficiency, in [36] has been improved by computing the patch distance with the subset of salient features associated with the pixels in contrast to averaging and weighing the pixels in nonlocal vicinities. The similarity between the pixels in the feature space is computed with the Least Square (LS) estimator by measuring the patch distances in the space of Taylor series coefficients. Reduction in computational cost in addition to an improvement in accuracy is observed. The problems associated with ultra-fast MRI acquisition and improving its computational efficiency is addressed by Naegel et al. [37]. In this paper, NLM filter is adapted to the context of real-time cardiac MRI. Redundancy between successive

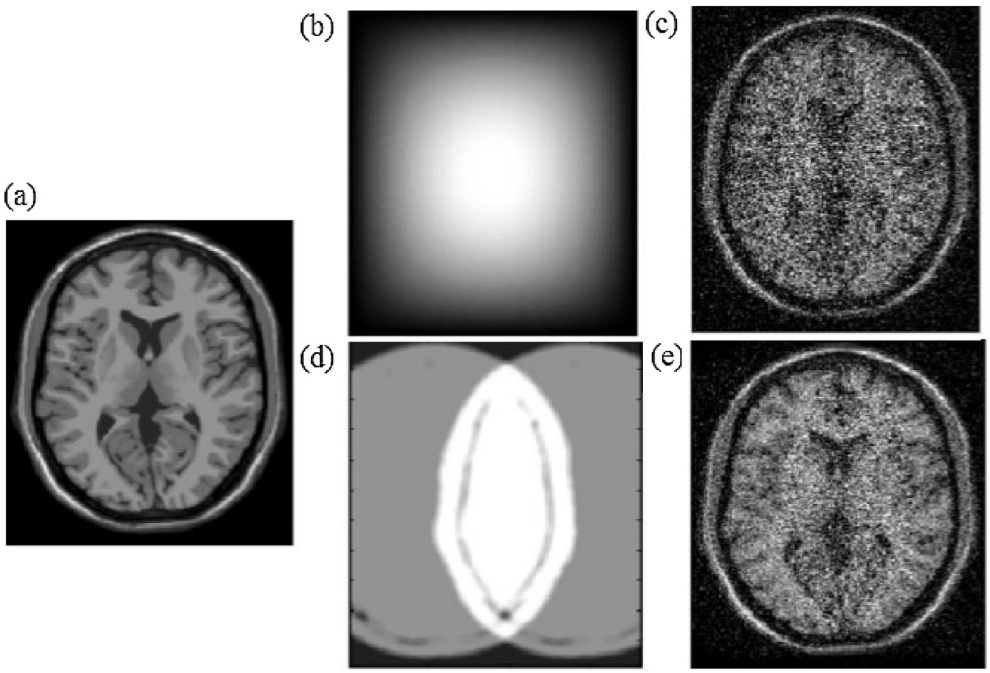

Fig. 2. Generation of noise maps for MR image a) original noise free image b) spatially slow varying noise modulation map c) resulting noisy image d) spatially fast varying noise modulation map and e) resulting noisy image (Ref. [42]).

frames is used to optimize the search space on recursive scheme having weights computed on filtered image. Computational burden is reduced by considering only similar patches in distance computations based on mean and variance as suggested in [38]. The techniques discussed so far are based on the assumption of spatial uniform noise distribution. However, the recent advances in parallel imaging in MRI lead to spatially non-uniform noise distribution as illustrated in Fig. 2. It is observed that fixing up the same patch size and search window irrespective of texture and noise variations in the MR image degrades the filter performance [39]. However, there are techniques where patch size and search window size is adaptively changed in accordance with the change in texture and noise variation to maximize the accuracy. Different variants of these have been categorized under adaptive NLM techniques.

3.2.2. Adaptive NLM techniques

An intrinsic property of any image including MR image is that its texture and noise varies at different locations. By choosing fixed filtering parameters such as search window, patch size and filtering coefficient the edges in the image may not be preserved well. And hence to maximize the accuracy, filtering parameters are changed adaptively depending on the local texture and noise variation. There are many papers in the literature which discuss these issues [39–53].

In [39] authors adapt the NLM filter based on the results of block classification. Block classification is performed with the technique of singular value decomposition that checks the dominant directions of edges in each block. Results of block classification are used to set the matching window size thus; the local property of the image is exploited. By adapting the size of the matching window in accordance with edge/textured regions, authors were able to improve the efficiency of the filter. However, this technique leads to more similar blocks and hence results in higher computations. For the efficient preservation of edge/textural patterns, in [40,41], NLM filter is adapted for local edge/ structural pattern by changing the weight function. In [40], σ value has been changed adaptively with a change in the local structure in the image. The accuracy of the filter is improved by selecting small σ values for highly edge/textured regions and large values for smooth regions. Thus σ varies with the edgeness parameter (E_i) given by

$$\sigma_i = \sigma\left(1 - \frac{E_i - E_{\min}}{E_{\max} - E_{\min}}\right) \tag{14}$$

where $E_{\min}$ and $E_{\max}$ denote the minimum and maximum edgeness values. Small σ_i value resulted due to high edgeness is able to change the patch similarity function adaptively resulting in the preservation of the original structure. Results are computed for Gaussian perturbed MR images however, the method suffers from high computational cost. Another NLM technique where the weighing term is adaptively changed in accordance with the edge/textured regions is discussed in [41]. In this work, LoG filter is used on Rician perturbed MR images to obtain the edge map. Similarity distances between the patches are computed for the edge map as

$$D_1 = ||LoG(N_i) - LoG(N_j)||_{2,\sigma} \tag{15}$$

where N_x is the patch and σ is the standard deviation. These similarity distances are combined with the intensity similarity while computing the weight function. The weighing term of NLM filter changes adaptively as edge pattern given by

$$w_m = \frac{1}{Z_i} e^{-\left(\frac{\left\|I(N_i)-I(N_j)\right\|^2_{2,\sigma}}{h^2}\right)-\left(\frac{\left\|LOG(N_i)-LOG(N_j)\right\|_{2,\sigma}}{h'}\right)} \tag{16}$$

Computational burden due to the additional edge term is reduced by preselecting the similar patches based on inverted mean and gradient measures. The technique discussed in [42] is in-line with [32] however, filter has been adapted for spatially varying noise. The technique relies on dividing the volumes into blocks with overlapping support. Restoration of voxel values depend on restored results of the blocks. The filter is adapted for spatially varying noise by estimating the noise locally instead of globally. Noise

estimation for spatially varying Gaussian perturbed MR image with self-similar patch is calculated as

$$\sigma^2 = \min\left(d\left(R_i, R_j\right)\right), \quad \forall i = j \quad \text{and} \quad R = u - \varphi(u) \tag{17}$$

where u is the original noisy volume and $\varphi(u)$ is the low-pass filtered volume. Due to low- pass filtering, the noise estimation changes to σ^2 from $\sigma^2/2$. Authors tried to adapt the filter for spatially varying Rician noise by applying low pass filter which provides a more regular estimation of the bias volume. However, it is observed that noise estimation underestimates on regions of low signal due to Rician nature of the noise however, a correction factor of local SNR as suggested by Koay and Basser [43] can be applied which is given by, $\sigma^2 = \sigma/\varepsilon(SNR)$ where $\varepsilon(SNR)$ is as explained in [43]. Krawtchouk moment employed as a similarity measure for patch distance computation is discussed in [44].

To preserve diagnostically important details and for local enhancement, similarity metric is redefined as [45]

$$w(i,j) = \frac{C\left(V(N_i),\, V\left(N_j\right)\right)}{2(i)} . e^{-\left(\frac{s\left(V(N_i), V(N_j)\right)}{h^2}\right)} \tag{18}$$

$$\text{where} \quad C(V_1, V_2) = \left\{ \begin{array}{ll} \dfrac{E(V_1)}{E(V_2)}, t_1 \neq t_2, & \left|E(V_1) - E(V_2)\right| > \sigma \\ 1 & \textit{Otherwise} \end{array} \right\} \tag{19}$$

Here t_1 and t_2 are temporal components from which vectors V_1, V_2 are selected, $E(V)$ is expected value. For noise perturbed MR images, NLM filter in-conjunction with anisotropic structure tensor is proposed by Wu et al. [46]. In this paper, the weight function is adapted by computing the patch similarity based on intensity and structure tensor simultaneously. Meanwhile, the similarity of the structure tensor is computed in a Riemannian space.

Papers [47,48], adapts weighing term of NLM filter in two ways. The first way is to select a few suitable pixels based on a robust threshold criterion. Second, a window adaptation technique is used based on the threshold value. A very similar strategy is used in [49,50] where weighing term or weighted sum is adapted by including additional voxels with the fact that human brain is complex and contains a lot of unique structures. In the former case, neighborhood size has been doubled by computing mid-sagittal plane which superposes the brain itself when mirrored about the plane whereas in the later, multiple scans are used to leverage the repeating structures from multiple MR images to collaboratively denoise an image.

Another paper where Rician noise has been removed by fuzzy similarity based NLM filter is suggested by Sharif et al [51]. Fuzzy similarity mechanism is constructed by Trapezoidal shaped function and fuzzy restoration is carried by modifying weight function, $w = e^{\frac{-(di,j-\mu)^2}{2\sigma^2}}$ where μ is the mean Gaussian function and $d_{i,j}$ is the Euclidean distance between patches. NLM filter with combined patch and pixel similarity is proposed by Zhang et al. [52]. In this work, particle preserving Rician NLM filter is proposed by calculating the weight with combined patch and pixel similarity. A vector based NLM scheme is proposed [53] by redefining the patch distance between neighborhoods of two vectors and is used for reliable estimation of diffusion kurtosis imaging using DWI data and redundant information acquired at different 'b' values.

3.2.3. NLM techniques on multiresolution / transform domain

MR image denoising with multiresolution technique was initially proposed by Weaver et al. [54]. Limited literature is available on multiresolution based NLM techniques. With the multiresolution framework, filtering parameters can be efficiently adapted over different spatial frequency resolution by combining filtered results with transform domain results. In [55], the intrinsic properties of MR image i.e., sparseness and self-similarity have been exploited for better denoising 3D MR images perturbed with Gaussian and Rician noises by using NLM technique in-conjunction with multiresolution. To reduce the computational time, speed-up strategy similar to [32] is used but with modification in patch distance computation. A statistically driven rule based technique is employed to compute the distance between the patches of the prefiltered volume. Hu et al. [56] worked on the similar principle to improve the filter efficiency by computing patch distances in Discrete Cosine Transform (DCT) subspace of neighborhood. Manjón et al. [42] adapted NLM filter for spatially varying noise, and further improved the performance of the filter by combining it with wavelet transform. This combined framework worked well to obtain the optimal set of parameters in space-frequency resolution for 3D MR data. Coupé et al. [57] proposed the multiresolution version of the blockwise NLM denoising technique to restore 3D MR images. The amount of denoising required is computed by estimating the noise level in accordance with spatial and frequency information of the image. To estimate the noise, adaptive soft wavelet mixing is carried out at the coefficient level of two denoised images; one image being adapted to the feature preservation and another to the noise component. Experiments are conducted on both Rician and Gaussian perturbed images. Authors [58] experimented on Rician perturbed MR images by adaptively changing the size of the search window in conjunction with wavelet coefficient mixing. Yang et al. [59] showed the efficacy of their technique by transforming the image by variance stabilizing transformation followed by pre-smoothing Rician noise perturbed MR images with the Gaussian filter. Computation of weights for NLM filter is carried with the smoothed image. Denoising with the combination of NLM and wavelet transform is proposed in [60]. Transforming an image into the domain of Neutrosophic Set (NS) authors [61] have applied wiener filtering on true and false sets. NS is applied in a post-filtering stage where three membership sets true, indeterminacy and false are defined. In [62], DCT is used as a smoothing kernel. Further, to suppress noise more efficiently NLM filter has been low pass filtered and similarity weights are calculated on a low dimensional version of neighborhood filter.

3.2.4. NLM techniques on statistical estimation

Most of the filters in this category use NLM principle for effective estimation of the noise in MR image as well as for patch distance computation in denoising. Estimation of noise is a necessary step for noise removal and also useful in the analysis of the MRI system. Lili et al. [63] and Jeny et al. [64,65] proposed nonlocal-maximum likelihood estimation (NL-MLE) approach to estimate Rician noise and employed nonlocal patch distance computations in denoising. These techniques were able to improve the efficiency of the NLM filter. MLE technique is deployed within nonlocal neighborhood to predict underlying noise-free signal by exploiting high degree of redundancy in the image content. Pixels with similar neighborhood are assumed from the same distribution thus, observations are located in the non-local neighborhoods for a given pixel to estimate its noise free value. These NL-MLE techniques result in over- smoothing or under-smoothing the images due to fixed sample size. The reason is being the fact that the samples for the ML estimation are selected in a nonlocal way based on the intensity similarity of the pixel neighborhood depending on Euclidean distance. However, these problems can be solved selecting the sample size in an adaptive way as suggested in [66]. The noise estimation and reconstruction process for aforementioned techniques are restricted for the MR images acquired with a single coil. Rajan et al. [67,68] extended the NL- MLE technique for MR images acquired with multiple coils. The methods are developed for non-central

Table 1
Summary of various NLM based MR image denoising techniques.

Denoising Technique	Advantages	Limitations
Fast NLM	Reduce the computational burden of NLM. Speed-up factor as high as 50 is achievable with parallelized computations	Degradation in the filters performance is observed especially at higher noise levels
Adaptive NLM	Improve filter efficiency by adapting the filtering parameters in-accordance with textural pattern, edge orientations and spatially varying noise	End up with higher computations and hence need to adopt speed-up strategy
Multiresolution/ transform domain based NLM	Possible to obtain optimal set of filtering parameters in space-frequency resolution	Need more refined scaling concepts. Cannot adapt to geometrical structure and may introduce characteristic artifacts
Statistical/ Estimation approach	Few techniques can estimate noise without background information, whereas few by changing the control parameters according to noise, thus improving filter performance	Can sometime overestimate or underestimate the noise level and hence over-smoothing or under- smoothing is observed

χ and spatially varying noise. These techniques are found to be effective on both simulated and real images however, some bias is observed in the resultant denoised image. NL-MLE technique in-conjunction with Kolmogorov –Smirnov (KS) similarity test provide better results as samples are selected in an adaptive and statistical way [69]. KS test is used to compare the distribution of patch distance ($D_{i,j}$) with standard normal distribution. Another NLM based LMMSE technique of denoising is suggested by Sudeep et al. [70]. In [71,72], NL- MLE and DCT techniques have been integrated to produce an improved MRI filtration process. A complete statistical interpretation of NLM filter is given by Thacker et al. [73]. In this paper, patch similarity and intensity weighing processes have been studied to a greater depth in terms of conventional statistics. Sudipto et al. [74] proposed a new similarity measure in patch distance computations for NLM filter by considering Rician statistics of the noise. A closed form expression corresponding to similarity measure is derived under the bonafide statistical assumption. Results are demonstrated for both in silico and in vivo MR data. Papers [75–77] are based on multivariate statistical technique such as Principal Component Analysis (PCA) for the accurate estimation of the covariance or correlation structure of the data to compute the correlated and uncorrelated set of data. Wood Kim et al. [75] worked on nonparametric PCA in-conjunction with NLM technique to denoise Rician perturbed MR images. Manjón et al. [76] for the first time developed a filter for multicomponent natured MR images using PCA technique. Filtering is done by spatial averaging of similar pixels using information from all available image components. To exploit the information from the inter-component domain and to remove noise, a local PCA technique is used. Gaussian noise simulated MR images are considered for experimentation however, authors have not proposed any speed-up strategy. Another NLM technique for spatially varying Rician noise using PCA decomposition is discussed in [77]. To adapt for spatially varying Rician noise, a non-local PCA decomposition with sliding window is used. The resulting filtered image is used intern to estimate voxel similarities within a rotationally invariant NLM filter. Multidimensional PCA in-conjunction with NLM filter for 3D MR data is proposed by Chang et al. [78]. A brief summary of advantages and limitations for the techniques discussed so far is provided in Table 1.

4. Results & discussion

In this section comparisons among various NLM based MR image denoising techniques are provided. Most of the work in the literature is based on Rician perturbed MR images acquired with single coil whereas quite a few on Gaussian perturbed MR images. Very limited literature is available on estimating the true signal value acquired with multiple coils. Performance of these techniques have been evaluated quantitatively and qualitatively with Peak Signal to Noise Ratio (PSNR), Structural Similarity Index Measure (SSIM), Universal Quality Index (UQI), Bhattacharya Coefficient (BC), Median Absolute Difference (MAD), Mean Square Error (MSE), Root Mean Square Error (RMSE), Mutual Information (MI), Contrast to Noise Ratio (CNR) and visual comparison. Manjón et al. [15] used RMSE and visual comparison as quality metrics to justify the superiority of their results. Authors in [32] have shown superior performance of their method with PSNR, BC, MI and residual images. For Rician perturbed images, authors [39] have used PSNR and visual comparison as performance metrics whereas in [41] authors have considered PSNR, SSIM, UQI, and BC as quantitative metrics. Authors in [42] have worked on parallel acquisition techniques like SENSE and GRAPPA that introduces spatially varying noise across the image and showed the superiority of their results with PSNR and residual image for both Rician and Gaussian perturbed images. Most of the literature [15,32,34,36,39,41] and [55–57,62,63,71] use synthetic data from brain-web database [79].

For comparative analysis, we consider T1 weighted, T2 weighted, and PD weighted MR axial volumes of size $181 \times 217 \times 181$ from brain web database [79]. Sample MR images used in our experiments are illustrated in Fig. 3. Experiments are demonstrated by simulating Rician noise for 9%, 11% and 15%. Here z% noise implies (z/100)*t, where t is the value of the brightest pixel in the image. To obtain maximum accuracy in each case, optimum filtering parameters are selected as suggested by the corresponding authors. Summary of which is provided in Table 2. The efficacy of various techniques is verified with wide variety of quality metrics such as PSNR, SSIM, UQI, BC and Contrast. In UQI, distortion in an image is modeled as a combination of loss of correlation, luminance distortion and contrast distortion [80] and hence is proved to be better than other widely used distortion

Table 2
Summary of optimal filter parameters for various NLM based MR image denoising techniques. S and N are radii of the search window and patch, respectively, h smoothing parameter, σ standard deviation of Rician noise.

Denoising Technique	Parameters
Fast biased nonlocal means (FBNLM) [33]	$S=5$, $N=2$, $h=\sigma$
Unbiased nonlocal means (UNLM) [15]	$S=5$, $N=2$, $h=\sigma$
Optimized blockwise nonlocal means (OBNLM) [32]	$S=5$, $N=2$, $h=\sqrt{2\beta\sigma^2\lvert V\rvert}$ where β is constant and $\lvert V\rvert$ is the number of voxels in the patch
Prefiltered rotationally invariant nonlocal means (PRI-NLM3D) [55]	$S=5$, $N=2$, $h=0.4\sigma$
Edge based adaptive nonlocal means(EANLM) [41]	$S=5$, $N=2$, $h=\sigma$
Adaptive blockwise nonlocal means (ABNLM) [42]	$S=3$, $N_1=1$, $N_2=2$, $h=\sigma$
Rotated block matching nonlocal means (RBNLM) [39]	$S=5$, $N=2$, $h=\sigma$
Adaptive multiresolution nonlocal means (AMNLM) [57]	$S=11$, $N=2$, $h=\sigma$

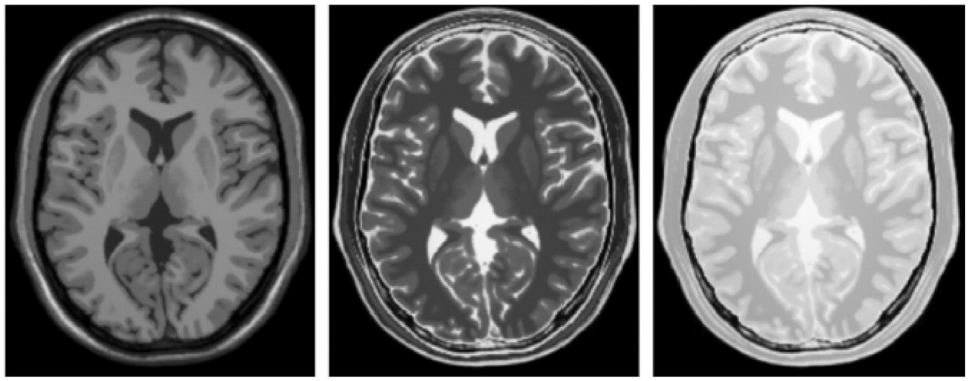

Fig. 3. Sample MR images used in the experimentation.

metrics. SSIM is used as a qualitative measure. Though PSNR is a commonly used objective metric, this does not match well with respect to the perceived quality [81]. SSIM within a local window is calculated as

$$SSIM(x,y) = \frac{\left(2\mu_x\mu_y + C_1\right)\left(2\sigma_{xy} + C_2\right)}{\left(\mu_x{}^2 + \mu_y{}^2 + C_1\right)\left(\sigma_x{}^2 + \sigma_y{}^2 + C_2\right)} \tag{20}$$

where x and y are the image patches extracted from the local window of the original and noisy images, respectively. $\mu_x, \sigma_x{}^2$, and σ_{xy} are the mean, variance, and cross-correlation computed within the local window, respectively. C_1 and C_2 are the constants as given in [82]. Finally, local SSIM is averaged to compute SSIM for the whole image.

Bhattacharya coefficient (BC) [83] measures distance between two histograms and treated as statistical measure for objective quality assessment. BC is given as

$$BC(k,l) = \sum_{b=0}^{255} \sqrt{k(b)\,l(b)} \tag{21}$$

where k and l are the two histograms of denoised and ground truth images, b is the bin index. BC value close to 1 indicates k and l being very similar. The bias introduced by Rician noise can significantly reduce the contrast between the tissues in MR images. To compare denoising techniques which restore the contrast between the tissues in MR images to the best possible extent, we compute contrast values as suggested in [18]. Let $\bar{I}_w$ and $\bar{I}_g$ be the mean intensity value in the region of white matter and gray matter in the denoised images. Then the equation for contrast between tissues is defined as

$$\text{Contrast} = \frac{1}{W} X \frac{\bar{I}_w - \bar{I}_g}{\bar{I}_w + \bar{I}_g} \tag{22}$$

where W is the normalization factor given by $W = \bar{m}_w - \bar{m}_g / \bar{m}_w - \bar{m}_g$. Here $\bar{m}_w$ and $\bar{m}_g$ are the mean intensity value in the region of white matter and gray matter in the noise free images.

The comparative results among various NLM based MR image denoising techniques are provided in Table 3. From the table, we can observe that the PSNR, SSIM and UQI values obtained with Fast Biased NLM (FBNLM) [33] method is least compared to all other methods. The reason is quite obvious. Authors have not provided any compensation for bias due to Rician noise. This paper basically aims to speed-up NLM filter so as to make it practically implementable. Manjón et al. [15] were the first among to compensate the bias introduced by Rician noise in NLM framework by subtracting the term $2\sigma^2$ from the denoised results. This technique is referred to as Unbiased NLM (UNLM) [15]. The obtained results are better compared to FBNLM which can be observed from the table; however, the filter is computationally slow. PSNR, SSIM and UQI values obtained with the technique Random Sampling with NLM (RSNLM) [34] are slightly inferior to UNLM. Results obtained with Non-Local means Maximum Likelihood Estimation technique (NLMLE) [63] are better than UNLM for all quality metrics mentioned. It is also observed from Table 3 that the Optimized Block-wise NLM (OBNLM) [32] technique provides the best results in addition to increased computational efficiency. However, lower efficiency is observed for Adaptive Blockwise NLM technique (ABNLM) [42] as authors have not provided any compensation for spatially varying noise. The Rotated Block matching NLM technique (RBNLM) [39] to search more number of similar blocks has resulted in improved performance w.r.t PSNR, SSIM and UQI values compared to Edge Adaptive NLM technique (EANLM) [41] however, the filter is computationally slow. Superior results are obtained for Prefiltered Rotationally Invariant NLM3D (PRI-NLM3D) [55] and Adaptive Multiresolution NLM3D (AMNLM3D) [57] techniques proposed by Manjón et al. which can be clearly observed from the Table 3. Both the techniques provide higher PSNR, SSIM, and UQI values compared to other techniques. For better performance in the former technique, authors have exploited sparseness and self-similarity properties of the image whereas, in the later NLM filter is adapted according to the spatial and frequency information in the image based on an adaptive soft wavelet coefficient mixing.

The graphs shown in Figs. 4 and 5 illustrate comparisons among various denoising techniques with respect to BC and Contrast values. From the Fig. 4, it is observed that the techniques EANLM and PRI-NLM3D provide relatively higher BC values compared to AMNLM3D and RBNLM. Higher BC values indicate that there is a strong correlation between the original and the denoised image. The least BC values are observed for FBNLM. Also from the Fig. 5 we can observe the contrast produced by AMNLM3D technique is superior compared to other techniques. The ability to restore contrast via the techniques PRI-NLM3D, RBNLM EANLM and OBNLM is better compared to RSNLM and UNLM. However, least performance is observed for FBNLM. In general, the ability to restore contrast drops for all the techniques as noise perturbation increases.

Comparative results for the run-time efficiency for various NLM based MR denoising techniques are illustrated in Table 4. For fair comparison, we have considered search window and patch window of sizes 11×11 and 5×5, respectively for all techniques. To compute the values of speed-up factor for various methods, original NLM [16] and UNLM techniques are considered as references. As UNLM and original NLM techniques require same runtime, values for original NLM are not provided in the table. Here we can note that the UNLM is the same NLM technique applied on MR dataset. From the table, higher computational efficiency is observed for PRI-NLM3D and OBNLM techniques compared to others. In PRI-NLM3D authors use statistically driven rule based on the distance between the patches of the prefiltered volume whereas for

Table 3
Quantitative performance comparisons among various NLM based MR image denoising techniques. The best values are indicated with bold numbers.

Denoising Technique	T1 weighted MR image 9% Rician noise			T2 weighted MR image 11% Rician noise			PD weighted MR image 15% Rician noise		
	PSNR	SSIM	UQI	PSNR	SSIM	UQI	PSNR	SSIM	UQI
FBNLM [33]	24.23	0.602	0.730	23.85	0.583	0.663	22.11	0.523	0.531
UNLM [15]	29.32	0.831	0.813	28.03	0.721	0.743	25.63	0.713	0.721
EANLM [41]	30.81	0.872	0.900	28.79	0.791	0.803	26.53	0.788	0.791
RBNLM [39]	31.74	0.898	0.929	29.31	0.823	0.842	27.06	0.821	0.823
OBNLM [32]	30.63	0.862	0.891	28.51	0.765	0.789	26.11	0.742	0.753
ABNLM [42]	25.38	0.653	0.781	24.98	0.643	0.701	22.41	0.542	0.561
AMNLM3D [57]	32.05	0.903	0.953	29.83	0.863	0.879	27.63	0.843	0.898
PRI- NLM3D [55]	**32.15**	**0.923**	**0.961**	**30.13**	**0.898**	**0.923**	**27.91**	**0.856**	**0.901**
RSNLM [34]	28.83	0.803	0.793	27.71	0.704	0.725	25.14	0.701	0.713
NLMLE [63]	30.53	0.863	0.873	28.54	0.763	0.767	26.05	0.753	0.769

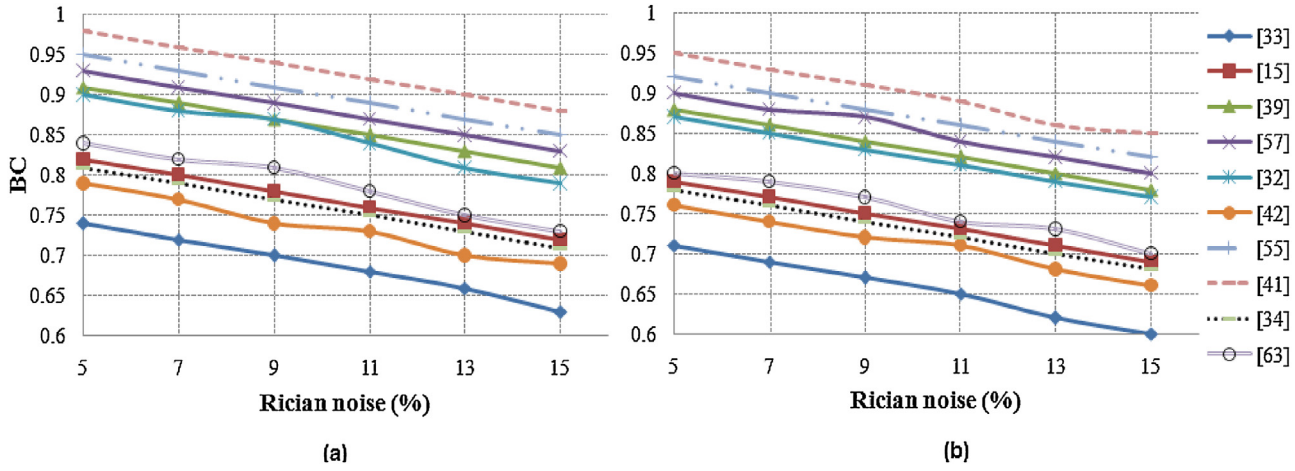

Fig. 4. Comparative plots of BC values for (a) T1 weighted and (b) T2 weighted MR image datasets.

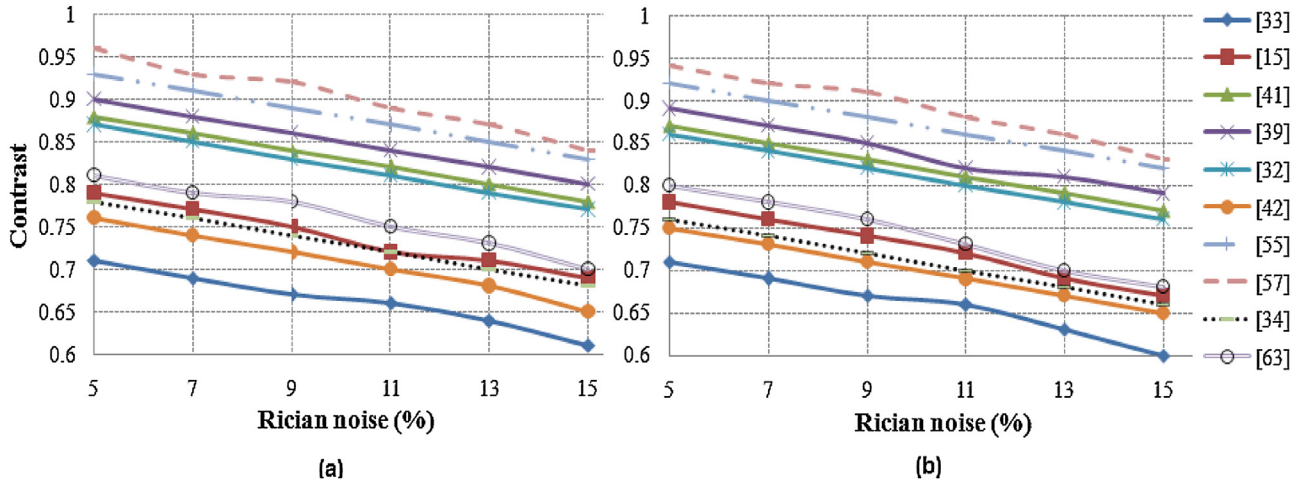

Fig. 5. Contrasts between white matter and gray matter on (a) T1 weighted and (b) T2 weighted MR image datasets.

OBNLM authors adopted the strategy of selecting only the relevant voxels and blockwise implementation. However, we have not carried out parallelized computations for any of these techniques. All experiments are carried out on a Dual Core Intel Pentium (R) D CPU 3.40 GHz processor. Both the techniques are more than 30 times faster than UNLM and original NLM method. However, computational time can be further reduced by parallelized computations. From the table, AMNLM3D and RSNLM techniques are observed to achieve faster results than [15,33,39,41]. The speed-up factor higher than 20 is achieved without compromising much on accuracy. Coupé et al. [33] method is observed to be providing a speed-up factor of 5.87 whereas [42], and [63] are 3.3 and 3.13 times faster than UNLM and original NLM methods. From the table, it is clearly observed that the computational efficiency achieved for EANLM [41] is lower than aforementioned methods as searching for similar patches are carried out separately for edge map and intensity map. To reduce the computational burden due to the additional edge term authors suggested inverted mean and gradient measure for the pre-selection of similar patches. This method is about 2.15 times faster than UNLM and original NLM methods. However,

Table 4
Run time (min) comparisons among various NLM based MR image denoising techniques (Speed-up factor is computed by considering UNLM technique as reference).

Denoising Technique	Runtime (min)	Speed-up factor
RBNLM [39]	25.0	0.42
UNLM [15]	10.45	1.00
OBNLM [32]	0.34	30.73
FBNLM [33]	1.78	5.87
EANLM [41]	4.84	2.15
RSNLM [34]	0.51	20.50
ABNLM [42]	3.16	3.30
PRI- NLM3D [55]	0.29	35.56
AMNLM3D [57]	0.41	25.53
NLMLE [63]	3.37	3.10

efficiency can be further improved by parallelized computations. From the table, it is observed that the run time requirement for both UNLM [15] and RBNLM [39] methods is quite high as these techniques are not supported with any speed-up strategies. Moreover, RBNLM method adopts rotated block matching strategy to improve the filter accuracy. The computational cost of this filter is about 2.39 times higher than the original NLM and UNLM methods. MATLAB codes for several NLM techniques are available on http://personales.upv.es/jManjón/denoising/arnlm.html.

5. Conclusions

The aim of this paper is to provide an exhaustive review of MR image denoising in a NLM framework. MR acquisition process introduces thermal noise in the images affecting human interpretation and computer-aided analysis. However, application of NLM filter in a post- acquisition process is observed to retain anatomical details of MR images with good accuracy. There are numerous NLM based MR denoising techniques which have been published till today which are summarized in this paper under the categories of Fast NLM, Adaptive NLM, multiresolution and statistical based NLM techniques. Also, we have discussed the advantages and limitations of each technique.

This paper compares various NLM based MRI denoising techniques with respect to their performance and run-time. Quantitative analysis has been provided with a wide number of performance metrics such as PSNR, SSIM, UQI, BC and Contrast. The PRI- NLM3D technique provides superior accuracy with respect to PSNR, SSIM, UQI measures with reduced computational time. EANLM technique provides the best BC values whereas, Contrast produced by AMNLM3D technique is superior. It is also observed that accuracy for the images acquired with parallel imaging and multiple coil systems is low as these approaches introduce spatially varying noise across the image. To deal with such noise, the denoising procedure requires a priori knowledge of the noise map. It is observed that no single NLM denoising method is available to deal with a wide variety of MR images perturbed with different kind of noise distribution. Also, no single method can be said to perform superior regarding noise reduction, edge preservation, robustness and computational cost. The aim of this review paper is to provide an overall view of available NLM techniques pertained to MR images which will help for the research community to choose the suitable denoising technique for their application or to develop the best denoising technique that overcomes limitations mentioned in thepaper.

References

[1] H. Gudbjartsson, S. Patz, The Rician distribution of noisy MRI data, Magn. Reson. Med. 34 (1995) 910–914.
[2] O. Dietrich, J.G. Raya, S.B. Reeder, M.F. Reiser, S.O. Schoenberg, Measurement of signal-to-noise ratios in MR images: influence of multichannel coils, parallel imaging, Magn. Reson. Imaging 2 (6) (2007) 375–385.
[3] O. Dietrich, J.G. Raya, S.B. Reeder, M. Ingrisch, M.F. Reiser, S.O. Schoenberg, Influence of multichannel combination, parallel imaging and other reconstruction techniques on MRI noise characteristics, Magn. Reson. Imaging 26 (2008) 754–762.
[4] P. Thunberg, P. Zetterberg, Noise distribution in SENSE and GRAPPA reconstructed images; a computer simulation study, Magn. Reson. Imaging 25 (2007) 1089–1094.
[5] J. Ashburner, K.J. Friston, Voxel based morphometry-the methods, Neuroimage 11 (2000) 805–821.
[6] E.R. Mcveigh, R.M. Henkelman, M.J. Bronskill, Noise and filtration in magnetic resonance imaging, Med. Phys. 12 (1985) 586–591.
[7] G. Gerig, O. Kubler, R. Kikinis, F.A. Jolesz, Nonlinear anisotropic filtering of MRI data, IEEE Trans. Med Imaging 11 (1992) 221–232.
[8] K. Murase, Y. Yamazaki, M. Shinohara, K. Kawakami, K. Kikuchi, H. Miki, T. Mochizuki, J. Ikezoe, An anisotropic diffusion method for denoising dynamic susceptibility contrast-enhanced magnetic resonance images, Phys. Med. Biol. 46 (2001) 2713–2723.
[9] A. Pizurica, W. Philips, I. Lemahiev, M. Acheroy, A versatile wavelet domain noise filtration technique for medical imaging, IEEE Trans. Med. Imaging 22 (2003) 323–331.
[10] D. Van De Ville, M. Seghier, F. Lazeryras, T. Blu, M. Unser, WSPM: wavelet based statistical parametric mapping, Neuroimage 37 (2007) 1205–1217.
[11] P. Saint-Marc, J.-S. Chen, G. Medioni, Bilateral spatial filtering: refining methods for localizing brain activation in the presence of parenchymal abnormalities, Neuroimage 33 (2006) 564–569.
[12] G. Hamarneh, J. Hradsky, Bilateral filtering of diffusion tensor magnetic resonance images, IEEE Trans. Image Process. 16 (2007) 1723–1730.
[13] M. Lie'vin, F. Luthon, E. Keevi, Entropic estimation of noise for medical volume restoration, Pattern Recognit. 3 (2002) 871–874.
[14] J. Ling, A.C. Bovik, Smoothing low- SNR molecular images via anisotropic median diffusion, IEEE Trans. Med. Imag 21 (2002) 377–384.
[15] J.V. Manjón, J. Carbonell-Caballero, J.J. Lull, G. Garcia-Mart, L. Mart-Bonmati, M. Robles, MRI denoising using non-local means, Med. Image Anal. 12 (2008) 514–523.
[16] A. Buades, B. Coll, J.M. Morel, A non-local algorithm for image denoising, IEEE Comput. Visual Pattern Recognit. 2 (2005) 60–65.
[17] R.M. Henkelman, Measurement of signal intensities in the presence of noise in MR images, Med. Phys. 12 (1985) 232–243.
[18] R.D. Nowak, Wavelet-based Rician noise removal for magnetic resonance imaging, IEEE Trans. Image Process. 8 (1999) 1408–1419.
[19] N. Otsu, A threshold selection method from gray-level histograms, IEEE Trans. Syst. Man Cybern. 9 (1979) 62–66.
[20] J. Sijbers, A.J. den Dekker, J.V. Audekerke, M. Verhoye, D. Van Dyck, Estimation of the noise in magnitude MR images, Magn Reson Imag 16 (1998) 87–90.
[21] J. Sijbers, A.J. den Dekker, P. Scheunders, D. Van Dyck, Maximum likelihood estimation of Rician distributed parameters, IEEE Trans Med Imag 17 (1998) 357–361.
[22] J. Sijbers, A.J. den Dekker, Maximum likelihood estimation of signal amplitude and noise variance for MR data, Magn. Reson. Imaging 51 (2004) 586–594.
[23] J. Sijbers, D. Poot, A.J. den Dekker, W. Pintjenst, Automatic estimation of the noise variance from the histogram of a magnetic resonance image, Phys. Med. Biol. 52 (2007) 1335–1348.
[24] S. Aja-Ferna'ndez, C.A. Lopez, C.F. Westin, Noise and signal estimation in magnitude MRI and Rician distributed images, a LMMSE approach, IEEE Trans. Image Process. 17 (8) (2008) 1383–1398.
[25] S. Aja-Ferna'ndez, G.V. Ferrero, Trista'n-Vega, Noise estimation in parallel MRI: GRAPPA and SENSE, Magn. Reson. Imaging 32 (3) (2014) 281–290.
[26] V. Brion, C. Poupon, O. Riff, S. Aja-Ferna'ndez, A. Trista'n-Vega, J.F. Mangin, D. Le Bihan, F. Poupon, Noise correction for HARDI and HYDI data obtained with multi channel coil and sum of square construction: an anisotropic extension of the LMMSE, Magn. Reson. Imaging 32 (3) (2013) 281–290.
[27] S. Aja-Ferna'ndez, V. Brion, A. Trista'n-Vega, Effective noise estimation and filteringfrom correlated multiple coil MR data, Magn. Reson. Imaging 31 (2013) 272–285.
[28] S. Aja-Ferna'ndez, A. Trista'n-Vega, C. Alberola-Lo'pez, Noise estimation in singleand multiple coil magnetic resonance data based on statistical models, Magn. Reson. Imaging 27 (2009) 1397–1409.
[29] N. Wiest-Daessle', S. Prima, P. Coupé, S.P. Morrissey, C. Barillot, Rician noise removal by non-local means filtering for low signal-to-noise ratio MRI:applications to DT-MRI, Med. Imaging Comput. Assist. Interv. (2008) 171–179.
[30] S. Aja-Fernandez, K. Krissian, An unbiased non-local means scheme for DWI filtering, Proc. Med. Imaging Comput. Comput. Assist. Interv. (2008) 277–284.
[31] N. Wiest-Daesslé, S. Prima, P. Coupé, S.P. Morrissey, C. Barillot, Non-local means variants for denoising of diffusion-weighted and diffusion tensor MRI, Med. Imaging Comput. Comput. Assist. Interv. (2007) 344–351.
[32] P. Coupé, P. Yger, S. Prima, P. Hellier, C. Kervrann, C. Barillot, An optimized blockwise nonlocal means denoising filter for 3-D magnetic resonance images, IEEE Trans. Med. Imaging 27 (2008) 425–441.
[33] P. Coupé, P. Yger, C. Barillot, Fast non local means denoising for 3D MR images, Med. Imaging Comput. Comput. Assist. Interv. (2006) 33–40.
[34] J. Hu, J. Zhou, X. Wu, Non-local MRI denoising using random sampling, Magn. Reson. Imaging 34 (2017) 990–999.

[35] H. Liu, C. Yang, N. Pan, E. Song, R. Green, Denoising 3D MR images by the enhanced non-local means filter for Rician noise, Magn. Reson. Imaging 28 (2010) 1485–1496.
[36] A. Trista'n-Vega, G.P. Veronica, S. Aja-Ferna'ndez, C.F. Westin, Efficient and robust non-local means denoising of MR data based on salient features matching, Compuy. Meth. Prog. Biomed. (2012) 131–144.
[37] B. Naegel, A. Cernicanu, J.N. Hyacinthe, M. Tognolini, SNR enhancement of highly accelerated real time cardiac MRI acquisitions based on nonlocal means algorithm, Med. Imaging Anal. 13 (2009) 598–608.
[38] M. Mahmoudi, G. Sapiro, Fast image and video denoising via nonlocal means of similar neighbourhoods, IEEE Signal Process. Lett. 12 (2005) 839–842.
[39] T. Thaipanich, C.C. Kuo, An adaptive nonlocal means scheme for medical image denoising, Proc. SPIE 7623 (2010) 1–12.
[40] B. Kang, O. Choi, J.D. Kim, D. Hwang, Noise reduction in magnetic resonance images using adaptive non-local means filtering, IEEE Electron. Lett. (2013) 49–55.
[41] H. Bhujle, S. Chaudhuri, Laplacian based nonlocal means denoising of MR image with Rician noise, Magn. Reson. Imaging 31 (2013) 1599–1610.
[42] J.V. Manjón, P. Coupé, L. Mart-Bonmat, D.L. Collins, M. Robles, Adaptive non-local means denoising of MR images with spatially varying noise levels, J. Magn. Reson. Imaging 31 (2010) 192–203.
[43] C.G. Kaoy, P.J. Besser, Analytically exact correction scheme for signal extraction from noisy magnitude MR signals, J. Magn. Reson. Imaging 179 (2006) 317–322.
[44] Ahlad Kumar, Nonlocal means denoising using orthogonal moments, Appl. Opt. 54 (27) (2015) 8156–8165.
[45] Y. Gal, A.J. Mehnert, A.P. Bradley, K. McMahon, D. Kennedy, S. Crozier, Denoising of dynamic contrast enhanced MR images using dynamic nonlocal means, IEEE Trans. Med. Imaging 29 (2009) 302–310.
[46] X. Wu, S. Liu, M. Wu, H. Sun, J. Zhou, Q. Gang, Z. Ding, Non-local denoising using anisotropic structure tensor for 3D MRI, Med. Phys. 40 (2013), 101904, http://dx.doi.org/10.1118/1.4820370.
[47] M. Aksam, A. Jalil, S. Rathode, A. Ali, M. Hussain, Brain MRI denoising and segmentation based on improved adaptive nonlocal means, Intl. J. Imaging Syst. Technol. 23 (2013) 235–248.
[48] M. Aksam, A. Jalil, S. Rathode, M. Hussain, Robust brain MRI denoising and segmentation using enhanced nonlocal means algorithm, Intl. J. Imaging Syst. Technol. 24 (2014) 52–66.
[49] S. Prima, O. Commowick, Using bilateral symmetry to improve non-local means denoising of MR brain images, Intl. Symon Biomed. Imaging (ISBI) (2013) 1231–1234.
[50] G. Chen, P. Zhang, Y. Wu, et al., Denoising magnetic resonance images using collaborative non-local means, Neurocomputing 177 (2016) 215–227.
[51] Muhmad Sharif, Ayyaz Hussain, Arfan Jaffar, Tae-Sun choi, Multimed. Tools Appl. 74 (July (15)) (2015) 5533–5556.
[52] X. Zhang, G. Hou, J. Ma, W. Yang, B. Lin, Y. Xu, et al., Denoising MR images using Non-local means filter with combined patch and pixel similarity, PLoS One 9 (6) (2014), e100240.
[53] M.X. Zhou, X. Yan, H.B. Xie, H. Zhang, D. Xu, G. Yang, Evaluation of nonlocal means based denoising filters for Diffusion Kurtosis Imaging using a new Phantom, PLoS One 10 (2) (2015), e0116986.
[54] J.B. Weaver, Y. Xu, D.M. Healy, L.D. Cromwell, Filtering noise from images with wavelet transforms, Magn. Reson. Med. 21 (1991) 288–295.
[55] J.V. Manjón, P. Coupé, A. Baudes, D.L. Collins, M. Robles, Med. Imaging Anal. 16 (2012) 18–27.
[56] J. Hu, Y. Pu, X. Wu, Y. Zhang, Improved DCT based non-local means filter for MR images denoising, Compt. Math. Meth. Med. 14 (2012), 232685.
[57] P. Coupé, J.V. Manjón, M. Robles, D.L. Collins, Adaptive multiresolution nonlocal means filter for 3D MR image denoising, IET Imag Process 6 (2012) 558–568.
[58] A. Jalil, S. Rathode, A. Ali, M. Hussain, An extended nonlocal means algorithm: application to brain MRI, Intl. J. Imaging Syst. Technol. 24 (2014) 293–305.
[59] J. Yang, J. Fan, D. Ai, S. Zhou, S. Jang, Y. Wang, Brain MR image denoising for Rician noise using pre-smooth nonlocal means filter, Biomed. Eng. Online 14 (2) (2015).
[60] P. Coupe, P. Hellier, S. Prima, C. Kervrann, C. Barrillot, 3D wavelet subbands mixing for image denoising, Intl. J. Biomed. Imaging (2008) 590183.
[61] J. Mohan, V. Krishnaveni, G. Yanhui, MRI denoising using nonlocal neutrosophic set approach of Wiener filtering, Biomed. Sign Process. Control 8 (2013) 779–791.
[62] X. Zheng, J. Hu, J. Zhou, MR image denoising using DCT-based unbiased non-local means filter, Proc. vol 8768, Intl. Conf on Graphics and Image proc, 2012.
[63] H. Lili, I.R. Greenshields, A nonlocal maximum likelihood estimation method for Rician noise reduction in MR images, IEEE Trans. Med. Imaging 28 (2009) 165–172.
[64] P.V. Sudeep, P. Palanisamy, Chandrasekharan Kesavadas, Jeny Rajan, An improved nonlocal maximum likelihood estimation method for denoising magnetic resonance images with spatially varying noise levels, Pattern Recognit. Lett. (2018), http://dx.doi.org/10.1016/j.patrec.2018.02.007.
[65] Adithya Upadhya, Basavaraj Talwar, Jeny Rajan, GPU Implementation of nonlocal maximum likelihood method for MRI denoising, J. Real Time Image Process. 13 (2017) 181–192.
[66] J. Rajan, J.V. Audekerke, A.V. der Linden, M. Verhoye, J. Sijbers, An adaptive nonlocal maximum likelihood estimation method for denoising magnetic resonance images, IEEE Intl. Sym. Biomed. Imaging (2012) 1136–1139.
[67] J. Rajan, J. Veraart, J.V. Audekerke, M. Verhoye, J. Sijbers, Nonlocal maximum likelihood estimation method for denoising multiple coil magnetic resonance images, Magn. Reson. Imaging 30 (2012) 1512–1518.
[68] J. Rajan, A.J. den Dekker, J. Juntu, J. Sijbers, A new non-local maximum likelihood estimation for denoising magnetic resonance images, Lecture notes in computer science, Springer, Berlic, Heidelberg, 2013, vol 8251.
[69] J. Rajan, A.J. den Dekker, J. Sijbers, A new nonlocal maximum likelihood estimation method for Rician noise reduction in magnetic resonance images using the Kolmogorov-Smirnov test, Signal Process 103 (2014) 16–23.
[70] P.V. Sudeep, P. Palaniswamy, C. Kesavadas, J. Rajan, Nonlocal linear minimum mean square error methods for denoising MRI, Biomed. Signal Process. Control 20 (2015) 125–134.
[71] S. Kumar, R. Ravindra, J. Rajan, L. Saba, J.S. Suri, Magnetic resonance image denoising using nonlocal maximum likelihood paradigm in DCT framework, Intl. J. Imaging Syst. Technol. 25 (2015) 256–264.
[72] P. Krishna kumar, P. Darshan, Sheetal Kumar, Rahul Ravindra, Jeny Rajan, Luca Saba, Jasjit S. Suri, Robust denoising MRI filter using nonlocal maximum likelihood paradigm in DCT framework, Int. J. Imaging Syst. Technol. 25 (2015) 256–264.
[73] N.A. Thacker, J.V. Manjón, P.A. Bromiley, Statistical interpretation of non-local means, IET Comput. Vis. 4 (2010) 162–172.
[74] S. Dolui, A. Kurstra, C. Ivan, S. Patarroyo, O.V. Michailovich, A new similarity measure for non-local means filtering of MRI images, J. Vis. Commun Imaging Rep. 24 (2013) 1040–1054.
[75] D. Wookkim, C. Kim, D. Heekim, D. Hoon Lim, Rician nonlocal means denoising for MR images using nonparametric principal component analysis, EURASIP J. Imaging Video Process. 1 (2011) 1–15.
[76] J.V. Manjón, N.A. Thacker, J.J. Lull, G. Garcia-Mart, L. Mart-Bonmati, M. Robles, Multicomponent MR image denoising, Intl. J. Imaging (2009) 756897.
[77] J.V. Manjón, P. Coupé, A. Baudes, MRI noise estimation and denoising using non-local PCA, Med. Imaging. Anal. 22 (2015) 32–45.
[78] Liu Chang, Gao Chao Bang, Yu Xi, A MRI denoising based on 3D non-local means and multidimensional PCA, Comput. Math. Methods Med. 232389 (2015).
[79] C.A. Cocosco, V. Kollokian, R.S. Kwan, A.C. Evans, Brain web: online interface to a 3D MRI simulated brain database, Neuroimage 5 (1997) S425 http://www.bic.mni.mcgill.ca/brainweb/.
[80] Z. Wang, A.C. Bovik, A universal image quality index, IEEE Signal Process. Lett. 9 (2002) 81–84.
[81] Z. Wang, A.C. Bovik, Mean squared error: love it or leave it? A new look at signal fidelity measures, IEEE Signal Process. Mag. 26 (2009) 98–117.
[82] H.R. Sheikh, E.P. Simoncelli, Z. Wang, A.C. Bovik, Image quality assessment: from error visibility to structural similarity, IEEE Trans. Image Process. 13 (2004) 600–612.
[83] A. Bhattacharyya, On a measure of divergence between two statistical populations defined by their probability distributions, Bull. Calcutta Math. Soc. 35 (1943) 99–109.